Article

Not peer-reviewed version

Experimental Evaluation of the Robust Controllers Applied on a Single Inductor Multiple Output DC-DC Buck Converter to Minimize Cross Regulation Considering Parametric Uncertainties and CPL Power Variations

Alvaro Christian Montaño Saavedra * , Walter Barra Junior , Renan Landau Paiva de Medeiros , Carlos Roozembergh Junior , Alan Sovano Gomes

Posted Date: 5 April 2024

doi: 10.20944/preprints202404.0433.v1

Keywords: Single inductor dual output DC-DC converter; parametric uncertainties; constant power load (CPL); linear quadratic regulator (LQR); integral square error; integral square control

Article

Experimental Evaluation of the Robust Controllers Applied on a Single Inductor Multiple Output DC-DC Buck Converter to Minimize Cross Regulation Considering Parametric Uncertainties and CPL Power Variations

Alvaro Christian Montaño Saavedra [1,*], Walter Barra Junior [1], Renan Landau Paiva de Medeiros [2], Carlos Roozenberg Junior [1] and Alan Sovano Gomes [1]

[1] Institute of Technology, Electrical Engineering Faculty, Federal University of Pará, 66075-110 Belém, PA, Brazil

[2] Department of Electricity, Federal University of Amazonas, 69080-900 Manaus, AM, Brazil; walbarra@ufpa.br (W.B.J.); renanlandau@ufam.edu.br (R.L.P.M.); carlos.silva.junior@itec.ufpa.br (C.R.J.); sovano@ufpa.br (A.S.G.)

* Correspondence: alvaromontano2009@gmail.com; Tel.: +55-11-93367-3582

Abstract: This paper presents two control design strategies for voltage regulation in a single inductor dual output (SIDO) DC-DC Buck converter system. Based on a nominal multiple input multiple output (MIMO) plant model and performance requirements, both an LQR and a decoupled PI control laws are designed to control the power converter system, under parametric uncertainties such as voltage source variation, CPL power variation, and load resistance variation. Therefore, the SIDO converter can cascade operating, which may cause the undesired effects of voltage oscillation and reduce the system's stability margin. The control performance was assessed under both uncertainties resistive loading and power variation of a constant power load (CPL). A SIDO DC-DC Buck converter board has been developed for experimental tests. The experimental results show that the LQR strategy, compared to the PI strategy, presented a robust performance in the presence of parametric uncertainties in the resistive loads being, however, sensitive to uncertainties due to the presence of CPL loads.

Keywords: single inductor dual output DC-DC converter; parametric uncertainties; constant power load (CPL); linear quadratic regulator (LQR); integral square error; integral square control

1. Introduction

Continued advances in control technology and power electronics have expanded the applications of power conversion systems in spacecraft, aircraft, ships, telecommunications networks, and electric vehicles, aiming to reduce size, weight, and cost, and to improve reliability, power quality, efficiency, and flexibility [1]. Some modern industries, whose processes require high dynamic performance, have used various types of power converters for applications, such as variable speed drivers [2], renewable energy systems [3,4], transportation systems [5,6], hybrid energy storage systems [7,8], and communication systems [9].

In several of these applications, switching power converters are controlled by PWM techniques to transfer power from a source to loads that typically have constant power characteristics. Because of the switching, the converters have some inherent nonlinear behaviors, such as high switching frequency, increasing harmonics in the system, current and voltage distortion, and instabilities that can occur due to these effects [10,11]. Therefore, it is a challenging task to ensure stability, transient performance, and higher efficiency of such converters.

 doi:10.20944/preprints202404.0433.v1

In order to reduce the weight reduction as well as to allow different regulated levels of DC voltage at the converter outputs, several studies [12–14] have recently proposed new converter topologies by sharing a single inductive element. One of the prominent topologies is the family of non-isolated DC-DC converters, i.e., single inductor multiple output (SIMO) DC-DC converters [15,16]. SIMO converters offer a good compromise in terms of the cost, efficiency, and diversity of potential applications. However, to operate effectively, a SIMO converter requires a high-performance control strategy, which leads to a number of challenging engineering problems, such as cross-regulation, high switching frequency, and severe nonlinearities. The main control challenge arises from the need (to reduce weight and cost) to share a single inductive element in a circuit. In short, a SIMO converter behaves similarly to a multivariable system with highly coupled loops, resulting in high dependencies between the main variables: the output voltages, coil current, and DC voltage gains [17].

Therefore, a complex automatic control system is required to maintain good performance regulation at different output voltage levels while minimizing the negative effects of the strong coupling between control loops. To this end, several studies have proposed solutions to mitigate coupling effects in DC-DC SIMO converters [12,15,18–24].

In other cases, a cascade of power electronic converters is a common feature of almost all converter-domain power systems to help provide the necessary load point regulation. However, tightly regulated electronic switching power converters act as constant power loads (CPLs) and tend to destroy the stability of power systems and upstream converters [25,26]; therefore, CPL can affect the power quality of the power systems and cause its instability and may eventually lead to system failure [27,28].

Despite the many advantages of DC power systems, ensuring their robust stability and performance remains an important technical challenge. This is mainly due to the non-linearities introduced by the CPL operation of the switching power converters and the non-linear characteristics of the converter itself. The problem is further aggravated by the interaction of different subsystems [29]. Therefore, the overall stability of the system cannot be guaranteed even if the individual subsystems are stable. It guarantees the analysis of the steady state and dynamic stability of the aggregated system under different loading curves.

Furthermore, most of the papers published so far have focused on mitigating the destabilizing effects of CPL without considering the uncertainty of the system parameters [30]. Therefore, there is still a lack of studies in the literature reporting robust parametric approaches for DC-DC converters driving CPLs to mitigate oscillation effects caused by CPL. The main contributions of this work are briefly summarized as follows:

- A decentralized robust control design methodology based on the LQR technique is described and applied to a multivariable dual-output DC-DC converter.
- A decentralized robust control design method based on the decoupled PID technique is described and applied to a multivariable dual-output DC-DC converter.
- The proposed methods are compared with one classical approach [31] to decentralized control. To this end, extensive experimental tests demonstrate the effects of different controllers, showing that the proposed LQR technique has better performance indices than other methods when the system is subjected to parametric variations (input DC voltage and resistance loads) and when a CPL is connected in each output once a time. Performance indices (ISE and ISU) are calculated to analyze the performance of the control method.
- For this purpose, a pilot plant (single inductor dual output DC-DC converter) was designed to implement the controllers and perform various tests to collect experimental data. The device allows the variation of physical parameters of the converter (input DC voltage and load resistances) and uses a programmable electronic load to emulate the behavior of the CPL.

The remainder of this article is organized as follows. Section II introduces the system description and problem formulation to solve the nonlinear analysis of the system; Section III briefly discusses the robust control methods proposed in this work. Section IV introduces the experimental

Preprints.org (www.preprints.org) | NOT PEER-REVIEWED | Posted: 5 April 2024 doi:10.20944/preprints202404.0433.v1

environment that describes the experiments to be performed in this paper; Section V discusses the result. Finally, the main conclusions are presented in Section VI.

2. System Description and Problem Formulation

2.1. Mathematical Model for a SIMO Converter

To represent the dynamic behavior of a single inductor multiple-output DC-DC converter system, the small-signal approximation model is adopted as an effective mathematical model [32]. Figure 1 shows a SIMO DC-DC converter with two outputs V_1 and V_2 and the topology used for the control system. The main feature of this converter is that the single inductor current I_L is split into two currents I_1 and I_2 at converter outputs 1 and 2 respectively. The uncertainties of the system are represented by arrows, i.e., loads and input voltage changes. These uncertainties often occur in real converters and affect performance. Therefore, control strategies must address this issue.

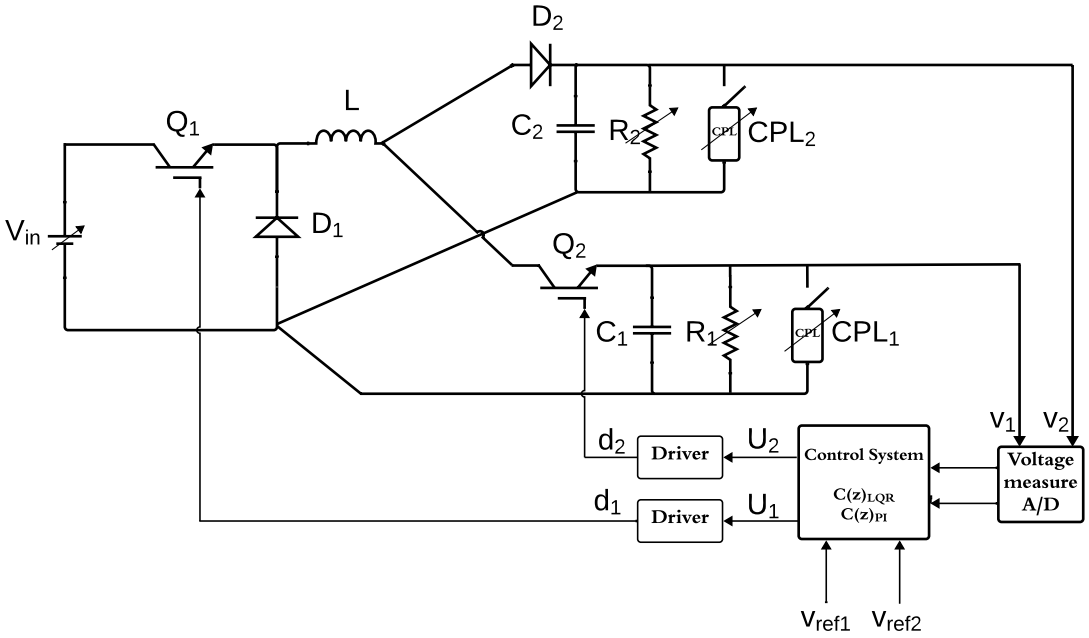

Figure 1. A two-output SIMO DC–DC buck converter system.

SIMO converters can be divided into three categories depending on the relationship between the duty cycle inputs d_1 and d_2, which control the MOSFET switches Q1 and Q2 (see Figure 1). In this study, a DC-DC SIMO converter operating according to Class-C (i. e. $d_1 < d_2$) is used [32]. In this case, the nonlinear average model of the converter is a third-order system given by the set of equations (1), whose state variables are the inductor current i_L and the voltages of the capacitors V_1 and V_2, and whose control inputs are the duty cycle of switches Q_1 and Q_2.

$$\begin{cases} L\frac{di_L}{dt} = V_{in}d_1 - V_1d_2 - V_2(1-d_2) \\ C_1\frac{dV_1}{dt} = i_Ld_2 - \frac{V_1}{R_1} \\ C_2\frac{dV_2}{dt} = i_L(1-d_2) - \frac{V_2}{R_2} \end{cases} \quad (1)$$

where V_{in} is the input unregulated voltage source value.

In the SIMO converter of Figure 1, the steady-state value D_1^0 of the duty cycle d_1 (switch Q_1) regulates the total input power and thus the coil current of the SIMO converter, while the steady-state value of the duty cycle d_2 (of switch Q_2), D_2^0, determines how the coil current is divided between the converter output loads R_1 and R_2. Assuming that the electronic switches and diodes are ideal, the components of the open-loop control-to-output 2x2 transfer function matrix at the operational point,

 doi:10.20944/preprints202404.0433.v1

$V_1^0, V_2^0, D_1^0, D_2^0, I_L^0$ and V_{in}^0, of the linearized model of the SIMO converter are given by the following formulas

$$g_{11}(s) = \frac{V_1(s)}{d_1(s)} = \frac{V_{in}^0 D_2^0 R_{eq1}}{(D_2^0)^2 R_{eq1} + (1-D_2^0)^2 R_{eq2} + sL} \quad (2)$$

$$g_{12}(s) = \frac{V_2(s)}{d_1(s)} = \frac{V_{in}^0 (1-D_2^0) R_{eq2}}{(D_2^0)^2 R_{eq1} + (1-D_2)^2 R_{eq2} + sL} \quad (3)$$

$$g_{21}(s) = \frac{V_1(s)}{d_2(s)} = \frac{I_L^0 R_{eq1}[(1-D_2^0)R_{eq2} + sL] + D_2^0 R_{eq1}(V_2^0 - V_1^0)}{(D_2^0)^2 R_{eq1} + (1-D_2^0)^2 R_{eq2} + sL} \quad (4)$$

$$g_{22}(s) = \frac{V_2(s)}{d_2(s)} = \frac{-[I_L^0 R_{eq2}(D_2^0 R_{eq1} + sL) + (1-D_2^0) R_{eq2}(V_2^0 - V_1^0)]}{(D_2^0)^2 R_{eq1} + (1-D_2)^2 R_{eq2} + sL} \quad (5)$$

where:

$$R_{eq1} = \frac{R_1}{1 + sC_1 R_1} \quad (6)$$

$$R_{eq2} = \frac{R_2}{1 + sC_2 R_2} \quad (7)$$

$$I_L^0 = \frac{V_1^0}{R_1} + \frac{V_2^0}{R_2} \quad (8)$$

For the study presented in this paper, the nominal values and assumed variation ranges for the SIMO converter circuit components are given in Table 1.

Table 1. DC – DC SIMO converter board test system parameters.

Parameter	Unit	Nom. Value	Variation	Description
V_{in}	V	7	[6-7]	Source input voltage
R_1	Ω	10	[5-10]	Loading at output 1
R_2	Ω	10	[5-10]	Loading at output 2
CPL_1	W	0.5	[0.6-0.5]	Output power of CPL_1
CPL_2	W	0.25	[0.35-0.25]	Output power of CPL_2
C_1	μF	2200	-	Capacitor at output 1
C_2	μF	1000	-	Capacitor at output 2
L	μH	330	-	Inductor
D_1^0	%	40	-	Operational point for duty cycle of output 1
D_2^0	%	60	-	Operational point for duty cycle of output 2
V_1^0	V	3.11	-	Operational point for output voltage 1
V_2^0	V	1.74	-	Operational point for output voltage 2
I_1^0	A	0.311	-	Operational point for current of the output 1
I_2^0	A	0.174	-	Operational point for current of the output 2
f_{sw}	kHz	7.8	-	Switching frequency
f_s	kHz	2.0	-	Sampling frequency

3. Proposals of Robust Controller Strategies for the SIMO Power Converter

3.1. Pairing Analysis for the SIMO Converter

The first step in the control design process is to perform a pairwise analysis to determine which output is most affected by a given plant input. There are several ways to do pairwise analysis in this topic. Nevertheless, the effective relative gain array (ERGA) is easy to implement and understand, and is more efficient than others arrays founded in the literature, e.g., relative gain array (RGA) or dynamic relative gain array (DRGA) [17].

The ERGA method is commonly used to determine the sensitivity of each output to each input. This procedure is provided by [33,34]. The main steps of the ERGA-based pairwise analysis are as follows.

1) Determine DC gain array using the DC gain for each element of the transfer function matrix.
2) Obtain the cutoff frequency for each element of the transfer function matrix.
3) Compute the energy transmission ratio array based on the DC gain and cutoff frequencies.
4) Compute the effective gains matrix that indicates the sensitivity between each I/O pair.
5) Compute the ERGA number and check for diagonal head dominance.

Preprints.org (www.preprints.org) | NOT PEER-REVIEWED | Posted: 5 April 2024 doi:10.20944/preprints202404.0433.v1

The effective gain matrix shown in (9) as a result of the ERGA pair analysis shows the optimal pairing, i.e., the first (V_1) and the second output (V_2) are respectively more sensitive to the first (d_1) and the second input (d_2).

$$\Phi = \begin{bmatrix} 0.762 & 0.238 \\ 0.238 & 0.762 \end{bmatrix} \quad (9)$$

Therefore, a simulation evaluation is performed to check the coupling between the system outputs. So first a pulse is applied to the duty cycle of switch Q1 and the system is run in open loop (without any controller) mode and then the same process is repeated for the switch Q2. Figure 2 shows the resulting coupling for the SIMO converter test system. The results show that V_2 is very sensitive to changes in duty cycle d_2, while V_1 is very sensitive to changes in duty cycle d_1. However, V_1 and V_2 are greatly affected by changes in d_1, although changes in d_2 don't have much relevant in the outputs of the system. This finding reflects the coupling between the loops of the system, which shows the efficient pairing of the ERGA analysis.

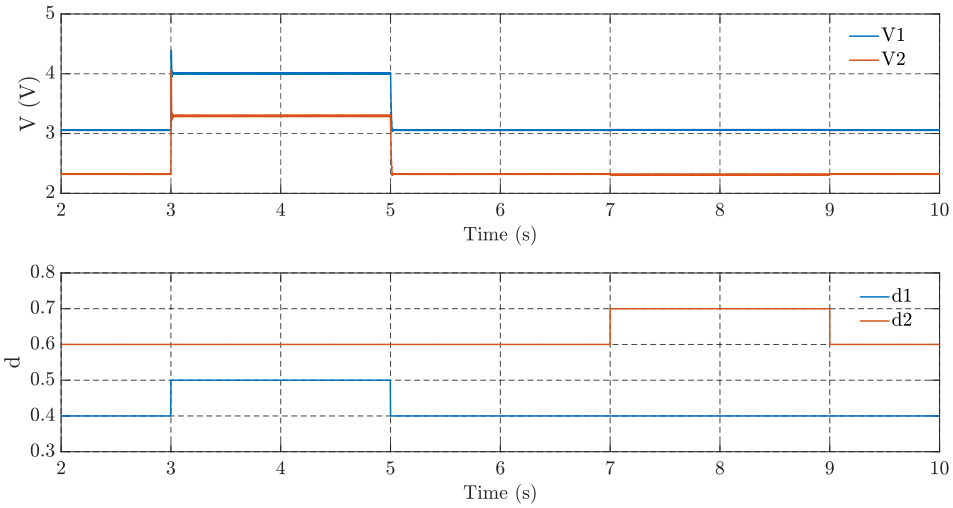

Figure 2. Simulation evaluation of switch duty cycle changes and corresponding output voltage variations.

3.2. Linear Quadratic Regulator Design

The LQR control is a well-known optimal-based approach to state feedback controller that can solve some problems in systems like instability or low stability margins, manipulating the system inputs and avoiding some typical problems on the stabilization problem like saturation control signal and fast actuator degradation [35]. This controller design is based on the choice of weight matrices of the states and control signal, Q and R respectively, which is used in the minimizing cost function.

$$J = \frac{1}{2}\sum_k^{\infty}(x(k)^T Q x(k) + u(k)^T R u(k)) \quad (10)$$

The minimization of the cost function results in a feedback control law.

$$u(k) = -R^{-1}B^T S x(k) \rightarrow u(k) = -Kx(k) \quad (11)$$

Positive-definite matrix "S" is a solution of the discrete-time algebraic Ricatti equation.

$$S = Q + A_d^T S A_d - A_d^T S B_d (B_d^T S B_d + R)^{-1} B_d^T S A_d \quad (12)$$

In this structure the LQR control on closed loop has not guaranteed perturbation reject in low frequency, however, this problem can be solved by an integrator addition on system input, creating a different model called "velocity model" [35]. The discrete integrator $\Delta = 1 - z^{-1}$ is inserted on the system plant, by this way creating a new state variable Δx(k).

$$\Delta x(k+1) = A_d \Delta x(k) + B_d \Delta u(k) \quad (13)$$

$$\Delta y(k) = C_d \Delta x(k+1) \quad (14)$$

Calling a new state vector $x_a(k) = [y(k)\ \Delta x(k)]^T$ and applying in the incremental model, the velocity model is presented.

Preprints.org (www.preprints.org) | NOT PEER-REVIEWED | Posted: 5 April 2024 doi:10.20944/preprints202404.0433.v1

$$\begin{bmatrix} y(k+1) \\ \Delta x(k+1) \end{bmatrix} = \begin{bmatrix} 1 & C_d A_d \\ 0 & A_d \end{bmatrix} \begin{bmatrix} y(k+1) \\ \Delta x(k+1) \end{bmatrix} + \begin{bmatrix} C_d B_d \\ B_d \end{bmatrix} \Delta u(k) \quad (15)$$

Inserting the augmented space state in the Ricatti transforms the feedback control law structure on a rejection perturbation problem.

$$u(k) = u(k-1) + K_y\, y_r(k) - K_{\Delta x} \Delta x(k) \quad (16)$$

Then the control law of the digital LQR for stabilization and perturbation reject problem is presented.

$$u(k) = u(k-1) + K_y\, y_r(k) - K_{\Delta x} \Delta x(k) \quad (17)$$

The Q and R weight matrices correct selection is important because it is responsible for the penalization of the dynamic states and input signal, respectively, in a way that Q and R inform the priority minimization order in the cost function, giving a trade-off balance between conflicting control objectives, such as minimizing control effort and regulation [36,37]. In this work, this selection is based on the loop-shaping of process singular values for improving robustness in high and low frequencies where stability Phase Margin, PM, and Gain Margin, GM, are used in the robustness design and bandwidth frequency is used in the converter velocity. This method is an interesting solution to controller's synthesis for Multiple Input Multiple Output process because of the difficulty in the frequency analysis in each loop [38]. For analysis of minimal stability margins (Phase Margin and Gain Margin) in the frequency singular values, the following constraints formulation, proposed in [39], is used:

$$GM_{dB} \geq 20 \log_{10} \min \left(\frac{m_s}{m_s - 1}, 1 + \frac{1}{m_t} \right) \quad (18)$$

$$PM_{deg} \geq \frac{180}{\pi} \times \min \left(2 \sin^{-1} \frac{1}{2m_s}, 2 \sin^{-1} \frac{1}{2m_t} \right) \quad (19)$$

where $m_s = max_\omega \sigma(S(j\omega))$ and $m_t = max_\omega \sigma(T(j\omega))$, with $max_\omega \sigma(T(j\omega))$ meaning the maximum singular value of a given transfer function matrix.

For LQR design purposes, assuming that the SIMO converter operates, in steady state, around operation point: $V_1^0 = 3.11\, V, V_2^0 = 1.74\, V, D_1^0 = 0.4, D_2^0 = 0.6, I_L^0 =$ 0.485 A and V_{in}^0 = 7 V. Then the corresponding matrices A, B, C and D of the linearized state-space model are:

$$A = \begin{bmatrix} -45.46 & 0 & 272.17 \\ 0 & -100.00 & 401.22 \\ -1814.50 & -1215.80 & 0 \end{bmatrix}, \; B = \begin{bmatrix} 0 & 172.09 \\ 0 & -378.60 \\ 21212.00 & -2266.70 \end{bmatrix} \quad (20)$$

$$C = \begin{bmatrix} 1 & 0 & 0 \\ 0 & 1 & 0 \end{bmatrix}, \; D = \begin{bmatrix} 0 & 0 \\ 0 & 0 \end{bmatrix}$$

By using the A, B, C and D matrices values given by (20), the corresponding open-loop transfer function matrix $G(s) = C(sI - A)^{-1}B + D$ has been computed. For discrete system model with sample time (ts=0.5 ms) the resulting maximum singular values for the sensitivity and complementary matrices transfer functions, S(z^{-1}) and T(z^{-1}), for the uncompensated closed-loop system (i. e., with an initial controller matrix $K_0 = I_{2x2}$) are presented in Figure 3.

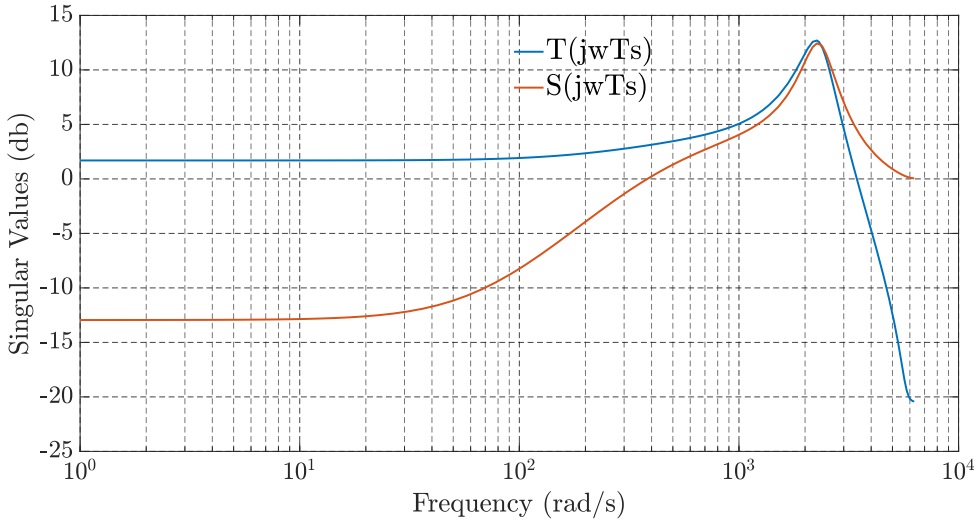

Preprints.org (www.preprints.org) | NOT PEER-REVIEWED | Posted: 5 April 2024 doi:10.20944/preprints202404.0433.v1

Figure 3. Maximum singular values of S(z^{-1}) and T(z^{-1}) for the uncompensated system.

$$S(z^{-1}) = (I_{2x2} + G(z^{-1}))^{-1},\ T(z^{-1}) = I_{2x2} - S(z^{-1}) \quad (21)$$

As can be seen, the maximum singular values for the sensitivity and complementary sensitivity transfer function matrices show very large peaks in high frequency, meaning that the uncompensated converter plant is very sensitive to high frequency noise and could become unstable due low attenuation property in high frequency band. Other problem, in this uncompensated plant, is its low capacity in tracking reference setpoint, due the reduced gain presented by T(s) at the low-frequency band. For this uncompensated system, the computed margins index shows low stability margins $GM_{dB} \geq 1.81$ and $PM_{deg} \geq 13.30°$, which confirms the singular values analysis.

For this case, low stability margins could be a problem, because uncertainty in circuit parameters (e.g., capacitors, inductors, and resistors) and in the input voltage are very common. Other problems are associated to noisy measurement (high frequency) and perturbations in low frequency. Aiming at improving the stability margins, the initial specified design requirements were: $GM_{dB} \geq 5$, $PM_{deg} \geq 45°$ and $\omega_{BT} \approx 200\, rad/s$, where ω_{BT} is the angular frequency such that the modulus of T(s=jω) is -3dB. By using the augmented state-space matrices given by (15), along with choosing weighting states and control matrices, $Q = diag(10, 10, 1000, 1000, 10)$ and $R = diag(10, 10)$, in LQR cost function (10), the computed value for the control vector gain was:

$$K = \begin{bmatrix} 0.0169 & -0.0055 & 0.0803 & -0.1003 & 0.0199 \\ 0.1059 & -0.0844 & 1.0188 & -0.7250 & -0.0435 \end{bmatrix} \quad (22)$$

The resulting maximum singular values for the sensitivity and complementary matrices transfer functions S(z^{-1}) and T(z^{-1}), for the compensated closed-loop system, are presented in Figure 4.

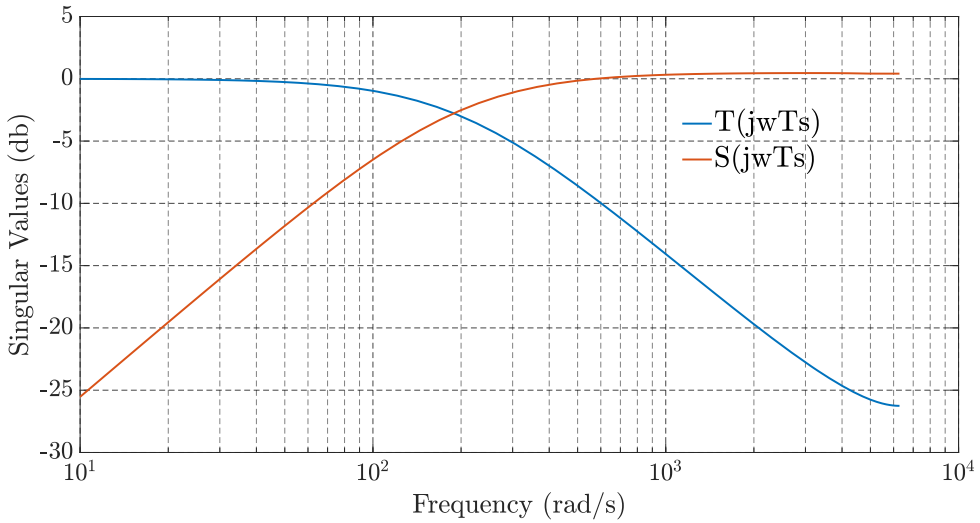

Figure 4. Maximum singular values of S(z^{-1}) and T(z^{-1}) for the compensated system.

As can be seen, in Figure 4, the computed controller is able to decrease the sensibility peaks which improve the process robustness. Furthermore, the perturbation rejection is also improved due to decreasing sensibility gain values in low frequency band. For this compensated system, the computed minimal stability margins and bandwidth frequency of the system are $GM_{dB} \geq 6.02$, $PM_{deg} \geq 56.62$ and $\omega_{BT} \approx 200\, rad/s$, which satisfy the design specifications.

3.3. Decoupled Multiloop PI Controller

The presentation is limited to two-input, two-output systems. Our approach was to explore standard PI multivariable (multi-loop) tuning [40] and observe what can be achieved by adding simple interactions between the feedback loops. The proposed scheme is based on a simple decoupling, which means that it can be easily implemented at the loop level [41]. The advantage is

Preprints.org (www.preprints.org) | NOT PEER-REVIEWED | Posted: 5 April 2024 doi:10.20944/preprints202404.0433.v1

that it improves performance in frequency ranges that modeling predictive control typically cannot handle.

The designable controller is a static decoupler combined with a decentralized PI controller with setpoint weighting. The control law can be written as:

$$\begin{pmatrix} U_1(s) \\ U_2(s) \end{pmatrix} = \begin{pmatrix} d_{11} & d_{12} \\ d_{21} & d_{22} \end{pmatrix} \begin{pmatrix} \bar{c_1}(s)Y_{r1}(s) - c_1(s)Y_1(s) \\ \bar{c_2}(s)Y_{r2}(s) - c_2(s)Y_2(s) \end{pmatrix} \quad (23)$$

where U is the control signal, Y the process output, and Y_r the reference. The decoupler:

$$D = \begin{pmatrix} d_{11} & d_{12} \\ d_{21} & d_{22} \end{pmatrix} \quad (24)$$

is a constant matrix. The PI controller $\bar{c_i}$ is different from c_i to allow for setpoint weighting [42]. The controllers are of the form:

$$c_i = k_{Pi} + \frac{k_{Ii}}{s} \quad (25)$$

$$\bar{c_i} = \frac{k_{Ii}}{s} \quad (26)$$

The static decoupler is given by:

$$D = G^{-1}(0) = \frac{1}{detG(0)} \begin{pmatrix} g_{22}(0) & -g_{12}(0) \\ -g_{21}(0) & g_{11}(0) \end{pmatrix} \quad (27)$$

where G(0) is non-singular. The transfer function of the decoupled system is given by:

$$q_{11}(s) = \frac{g_{11}(s)g_{22}(0) - g_{12}(s)g_{21}(0)}{detG(0)} \quad (28)$$

$$q_{12}(s) = \frac{g_{12}(s)g_{11}(0) - g_{12}(s)g_{11}(0)}{detG(0)} \quad (29)$$

$$q_{21}(s) = \frac{g_{12}(s)g_{22}(0) - g_{21}(s)g_{22}(0)}{detG(0)} \quad (30)$$

$$q_{22}(s) = \frac{g_{22}(s)g_{11}(0) - g_{21}(s)g_{12}(0)}{detG(0)} \quad (31)$$

A Taylor series expansion of the transfer function Q(s), for a small s, gives:

$$Q(s) \approx \begin{pmatrix} 1 & k_{12}s \\ k_{21}s & 1 \end{pmatrix} \quad (32)$$

for some constants k_{12} e k_{21}. Then it´s possible to introduce the interaction indices:

$$k_1 = |k_{12}k_{I2}|M_{s1}M_{s2} \quad (33)$$

$$k_2 = |k_{21}k_{I1}|M_{s1}M_{s2} \quad (34)$$

where M_{s1} and M_{s2} are the maximum sensitivities of each loop. The indices k_1 and k_2 describe the interaction between the loops. The indices are the result of two terms: one is system dependent and the other is directly the integral gain of the PI controller. Therefore, the interaction can be reduced by decreasing the controller gains [36]. To find the decentralized PI controllers, we need to consider the diagonal terms of Q(s). Hence, standard methods can be used to design the PI controllers for each transfer function $q_{kk}(s)$.

By considering the same operating point used for the design of the LQR controller ($V_1^0 = 3.11\,V, V_2^0 = 1.74\,V, D_1^0 = 0.4, D_2^0 = 0.6, I_L^0 =$ 0.485 A and V_{in}^0 = 7 V) the following values were computed for the transfer functions $g_{11}(s), g_{12}(s), g_{21}(s), g_{22}(s)$:

$$g_{11}(s) = \frac{5.773\times10^6 s + 5.773\times10^8}{s^3 + 145.5s^2 + 9.862\times10^5 s + 7.156\times10^7} \quad (35)$$

$$g_{12}(s) = \frac{8.511\times10^6 s + 3.868\times10^8}{s^3 + 145.5s^2 + 9.862\times10^5 s + 7.156\times10^7} \quad (36)$$

$$g_{21}(s) = \frac{172.1s^4 - 5.841\times10^5 s^3 + 9.337\times10^7 s^2 + 1.217\times10^{10} s + 3.048\times10^{11}}{s^5 + 236.4s^4 + 1.001\times10^6 s^3 + 1.615\times10^8 s^2 + 8.543\times10^9 s + 1.478\times10^{11}} \quad (37)$$

$$g_{22}(s) = \frac{-378.6s^4 - 1.002\times10^6 s^3 - 5.427\times10^8 s^2 - 7.999\times10^{10} s + 3.536\times10^{12}}{s^5 + 345.5s^4 + 1.025\times10^6 s^3 + 2.703\times10^8 s^2 + 2.417\times10^{10} s + 7.156\times10^{11}} \quad (38)$$

Thus, it's possible to determine the matrix static decoupler D by using (27), the computed value obtained of D was:

$$D = \frac{1}{-51.012} \begin{pmatrix} -4.941 & -5.406 \\ -2.062 & 8.068 \end{pmatrix}$$

$$D = \begin{pmatrix} 0.097 & 0.106 \\ 0.040 & -0.156 \end{pmatrix} \quad (39)$$

The transfer function of the decoupled system can be obtained considering the equations (28) to (31), hence, to design the decentralized PI controllers we have to consider the diagonal terms of Q(s):

$$q_{11}(s) = \frac{9.032\times10^5 s + 7.156\times10^7}{s^3 + 145.5s^2 + 9.862\times10^5 s + 7.156\times10^7} \quad (40)$$

$$q_{22}(s) = \frac{78.12s^3 + 8.655\times10^4 s^2 + 7.533\times10^7 s + 3.252\times10^9}{s^4 + 190.9s^3 + 9.928\times10^5 s^2 + 1.164\times10^8 s + 3.253\times10^9} \quad (41)$$

Preprints.org (www.preprints.org) | NOT PEER-REVIEWED | Posted: 5 April 2024 doi:10.20944/preprints202404.0433.v1

Therefore, for each transfer function $q_{11}(s)$ and $q_{22}(s)$, the root-locus design method for the PI controllers is used with the chosen requirements: settling time less than 0.5 s and damping factor greater than 0.2 (these nominal specifications give reasonable performance for DC-DC power converters [42]), the corresponding parameters were obtained:

$$k_{P1} = 0.87, k_{I1} = 30.0, k_{P2} = 14.5, k_{I2} = 500.0 \quad (42)$$

Thus, the corresponding transfer functions of the controllers PI_1 and PI_2 have the structures of the equations (25) and (26). Thus, the corresponding state-space representation is:

$$\begin{bmatrix} U_1(s) \\ U_2(s) \end{bmatrix} = \begin{bmatrix} -d_{11}k_{P1} & d_{11}k_{I1} & -d_{12}k_{P2} & d_{12}k_{I2} \\ -d_{21}k_{P1} & d_{21}k_{I1} & -d_{22}k_{P2} & d_{22}k_{I2} \end{bmatrix} \begin{bmatrix} Y_1(s) \\ X_{I1}(s) \\ Y_2(s) \\ X_{I2}(s) \end{bmatrix} \quad (43)$$

Where

$$X_{I1}(s) = \frac{E_1(s)}{s}, \quad X_{I2}(s) = \frac{E_2(s)}{s}, \; Y_1(s) = V_1(s), Y_2(s) = V_2(s) \quad (44)$$

Thereby, the control law equation can be represented like

$$U(s) = kCX(s) + k_I \frac{E(s)}{s} \quad (45)$$

Where

$$k = \begin{bmatrix} -d_{11}k_{P1} & -d_{12}k_{P2} \\ -d_{21}k_{P1} & -d_{22}k_{P2} \end{bmatrix}, k_I = \begin{bmatrix} d_{11}k_{I1} & d_{12}k_{I2} \\ d_{21}k_{I2} & d_{22}k_{I2} \end{bmatrix} \quad (46)$$

4. Experimental Methodology and Tests

4.1. Description of the SIMO Converter System Test Board

To allow the experimental performance and robustness evaluation of the proposed control methods, namely LQR and Decoupled PI (see Figure 1), a single-inductor dual-output DC-DC Buck converter board test system was developed. This test board (together with the measuring equipment) is shown in Figure 5. This test system was designed according to the specifications in Table 1. It allows two different levels of regulated DC voltage and allows for variations in the input voltage and loads converter outputs. A microcomputer system that communicates via USB is used to set the desired set point and to monitor and acquire converter relevant signals (i.e., voltages, inductor current and control efforts). Note that the special design of the power converter allows the circuit parameter values to be easily changed to emulate parametric uncertainties as well as changing operating conditions.

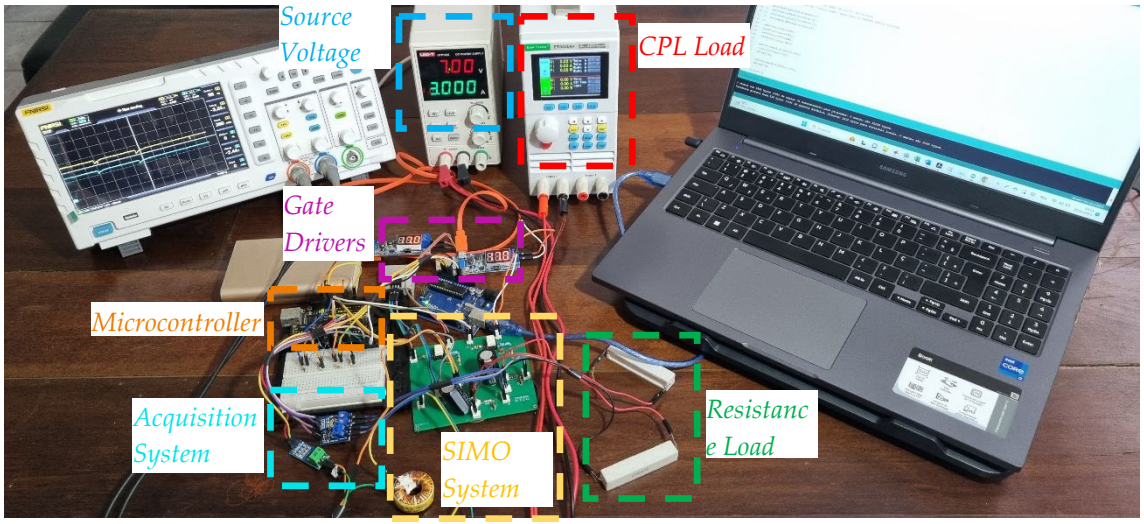

Figure 5. Overview of the single inductor multiple output DC-DC converter test system developed for the experimental tests.

 doi:10.20944/preprints202404.0433.v1

The SIMO test system (Figure 5) implements the control laws, LQR and Decoupled PI, by using vector and matrices structures in a 32-bit ARM core microcontroller AT91SAM3X8E, with the programming done by a C compiler.

In addition, two other subsystems have been developed for the use of parametric variations. The first allows performing variations on the input voltage value, while the second allows to change the load conditions of the converter using parallel addition (or deleted) resistances to the converter output, or by adding a CPL with variations in its power consumption. In addition, the microcomputer system uses an application that allows real-time visualization of data and recording of data for posterior analysis.

4.2. Description of Experiments

Tree experiments are performed to evaluate the performance and robustness of the real closed-loop SIMO converter system. The first experiment is designed to evaluate the controller performance for variations on the value of converter input voltage, V_{in}. With the system operating in steady state at the operating point provided in Table 1, a step variation was applied in Vin, from 7V to 6 V.

Remark 1. Note that it is not advisable to reduce the input voltage of the SIMO converter to a greater extent as it will reduce the inductor current, which would then change the operational conduction mode of the converter from the continuous to discontinuous conduction mode.

The second experiment evaluates the performance of the controller for a single variation of the load resistance R1 and R2 after the steady state is achieved at the nominal operation point, from R = 10 Ω to R = 5 Ω in each case.

Remark 2. Note that **the rig system's physical limits are limited by the maximum operation of the voltage source power, while the minimum operation is limited by the current level that maintains the operational conduction mode of the SIMO converter.**

The third experiment evaluates the closed-loop performance when the CPLs undergoes negative power variations in parallel with R1 and R2. When the SIMO converter system reaches its stable state, CPL1 is connected in parallel with R1 and after a few seconds a negative power change is given to CPL1 (CPL2 is not yet connected). The same procedure is adopted for the output voltage at R2. The exact values of the CPLs variations are described in Section 5.3.

The aim of these experiments is to show that the proposed controllers can compensate for the perturbations when the input voltage and load change, thereby maintaining the desired performance in the uncertainty region and at different operation points without increasing the measurement noise. The integral square error (ISE) and the integral square control (ISU) indices are used to evaluate the performance of the control strategies.

5. Experimental Results and Discussion

5.1. Input Voltage Variation

With the real SIMO converter test system (see in Figure 4), operating in steady state around the operating point ($V_1^0 = 3.7\ V, V_2^0 = 2.7\ V, d_1^0 = 0.7, d_2^0 = 0.7$), a negative step variation was applied on the value of the external converter input voltage, Vin, from 7.0 to 6.0 Volts, at the time instant t = 69.0. In Figure 6 are presented the acquired signals of output voltages, V_1 and V_2, as well as the corresponding control efforts, d_1 and d_2, provided by LQR and Decoupled PI controllers, respectively. As can be observed, both designed controllers, LQR and Decoupled PI, were able to ensure the system stability. However, only the LQR strategy have succeeded in compensates for the variation in Vin, by adequately regulating both outputs, V_1 and V_2, for their respective pre-disturbance values, without excessive control effort or saturation in both duty cycle signals d_1 and d_2, showing a good performance obtained by the LQR strategy. In contrast, Figure 6 also shows that the experimental results obtained for the Decoupled PI strategy, at the same test, was not satisfactory. Although the PI strategy was able to provides a stable closed-loop system, it fails in adequately regulate the voltage outputs V_1 and V_2 to their respective pre-disturbance values. A possible cause may reside in the

Preprints.org (www.preprints.org) | NOT PEER-REVIEWED | Posted: 5 April 2024 doi:10.20944/preprints202404.0433.v1

assumed degree of decoupling imposed in the PI design, which could be an excessive requirement. Further research is needed in this particular point.

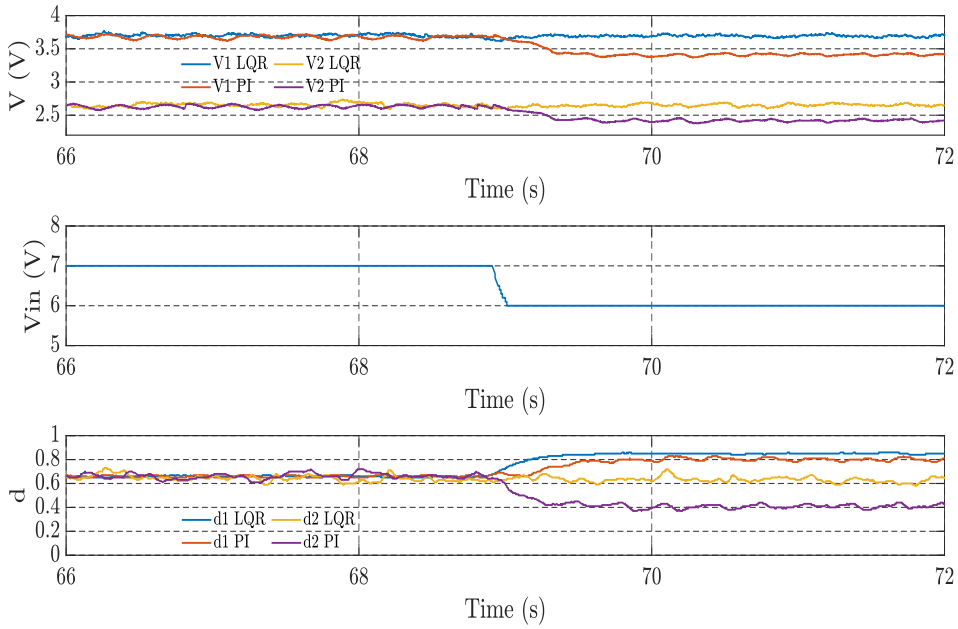

Figure 6. Experimental results for a step variation on the value of the input source voltage in the single inductor dual output converter system, using LQR strategy and Decoupled PI structure.

Table 2 shows the comparison of ISE and ISU performance indices for the single inductor dual output converter test system between two approaches.

Table 2. Values of the ISE and ISU indexes of the experimental data collected when the system submitted a parametric variation in input voltage.

Test	OUTPUT	ISE		ISU		J = ISE + ISU	
		LQR	PI	LQR	PI	LQR	PI
Vin	V1	0.00039	0.0368	0.5549	0.5227	0.5553	0.5595
	V2	0.0028	0.0355	0.4201	0.3211	0.4229	0.3566

Those evaluates the impact of voltage variation on the controller performance. In the case of the output V_1, it is possible to notice that ISE index value of the LQR strategy is almost one hundred times smaller in comparison with the decoupled PI index value. Furthermore, the ISU index values show that the improvement in the voltage regulation happened with less than 10 percent increase in the LQR ISU index in comparison with the PI ISU index. In the case of the output V_2, it is possible to notice that ISE index value of the LQR strategy is about ten times smaller in comparison with the decoupled PI index value. Moreover, the ISU index values show that the improvement in the voltage regulation happened with less than 30 percent increase in the LQR ISU index in comparison with the PI ISU index. Therefore, the preview analysis supports improving robustness of the proposed LQR control.

5.2. Load Variation

The load variation test is performed by changing the load at each converter output, keeping the value $V_{in} = 7$ V. The load resistance value at each converter output is gradually reduced by adding resistors in parallel with it. As a result, the corresponding output current value changes. Figure 7

 doi:10.20944/preprints202404.0433.v1

shows the closed-loop response of voltages V_1 and V_2 using LQR and Decoupled PI controllers, and the corresponding control efforts, d_1 and d_2. The system starts with a load resistance of $R_1 = 10\ \Omega$. At t = 90 s, a 10 Ω resistor is inserted in parallel, reducing the load resistance value to 5 Ω. It can be seen that only the controller method using the LQR strategy can effectively regulates the two outputs, V_1 and V_2 to reach their respective pre-disturbance values without excessive control effort or saturation of the duty cycle signals d_1 and d_2 and has a fast response. Furthermore, the Decoupled PI controller causes steady state errors mainly at V_1, and it can also be seen that V_1 is more affected because its more sensitivity to loop interactions.

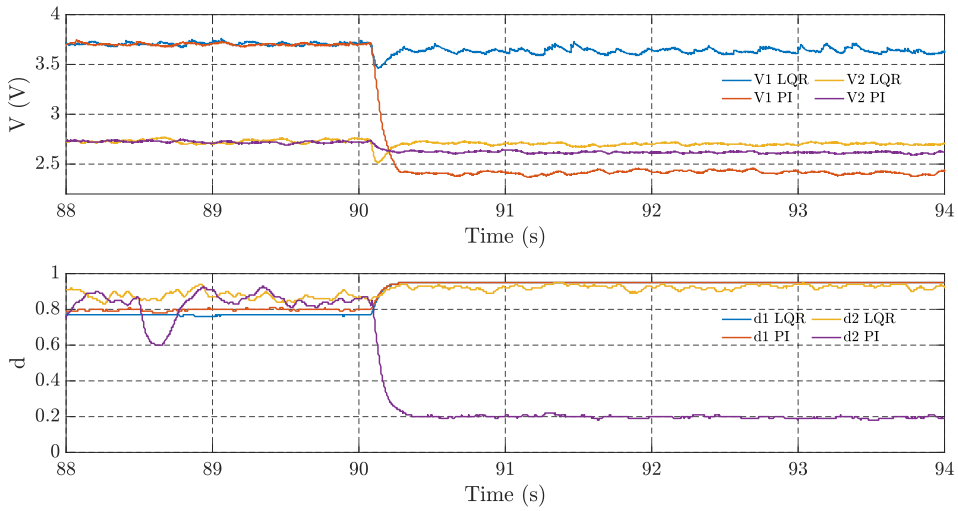

Figure 7. Experimental results for the test of load variation R1 in output 1 of the single inductor dual output converter system, using LQR strategy and Decoupled PI structure.

Similar results were obtained for the load variations in output 2 of the LQR strategy and the Decoupled PI control structure, as shown in Figure 8. However, the controller designed with the LQR strategy correctly compensated the oscillations due to load variation in output 2 of single inductor dual output converter. The results for outputs 1 and 2 were collected simultaneously for the same load variation, i.e., adding a 10 Ω resistor in parallel with the resistor $R_2 = 10\ \Omega$. The LQR strategy is capable of quickly compensating for the load variation, nearly eliminating steady-state error in V_1 and V_2 without saturating the control signals. On the other hand, the Decoupled PI controller method cannot compensate for the load variations at outputs 1 and 2, resulting in significant performance degradation, which is mainly reflected in output 2′s high steady-state error value.

Preprints.org (www.preprints.org) | NOT PEER-REVIEWED | Posted: 5 April 2024 doi:10.20944/preprints202404.0433.v1

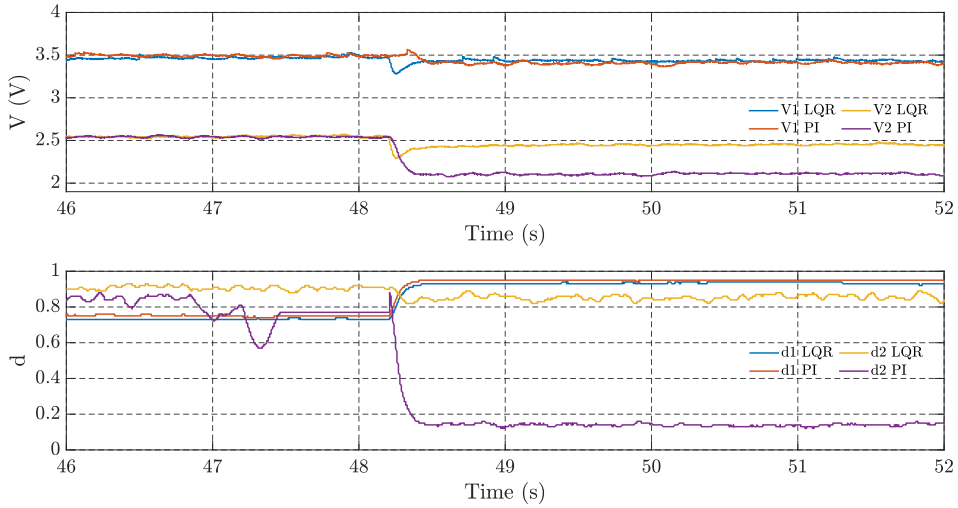

Figure 8. Experimental results for the test of load variation R2 in output 2 of the single inductor dual output converter system, using LQR strategy and Decoupled PI structure.

Table 3 shows the ISE and ISU indices for each output due to the load changes at output 1 for the LQR strategy and the Decoupled PI control structure. Compared to the Decoupled PI structure values, the ISE of the proposed LQR strategy is lower for both outputs. However, it can be seen that the ISU index value of the LQR case is much higher than in the Decoupled PI case, especially for output 2. Also, Table 4 shows the same index values for variations in output 2 for LQR strategy and Decoupled PI control structure. The proposed LQR strategy offers lower ISE values compared to the Decoupled PI values. These results show that the proposed LQR strategy provides significant performance improvements and justifies its application in single inductor dual output converter systems.

Table 3. Values of the ISE and ISU indexes of the experimental data collected when the system submitted a parametric variation in load R1.

Test	OUTPUT	ISE		ISU		J = ISE + ISU	
		LQR	PI	LQR	PI	LQR	PI
R1	V1	0.0036	0.8938	0.7614	0.7779	0.7649	1.672
	V2	0.0011	0.0042	0.8099	0.3336	0.8111	0.3378

Table 4. Values of the ISE and ISU indexes of the experimental data collected when the system submitted a parametric variation in load R2.

Test	OUTPUT	ISE		ISU		J = ISE + ISU	
		LQR	PI	LQR	PI	LQR	PI
R2	V1	0.0637	0.0638	0.7023	0.7360	0.7660	0.7998
	V2	0.0443	0.1881	0.7758	0.3343	0.8201	0.5223

5.3. CPL Power Variation

The CPL power variation test is performed by placing the CPL in parallel with the load resistor and varying its power value at each output of the converter. The load resistance value at each converter output is fixed at 10 Ω. By using a Programmable DC Electronic Load in parallel with each resistor, the CPL power value at each output of the converter is gradually increased. As a result, the corresponding output current value is changed. Figure 9 shows the closed-loop response of the V_1 voltage using the LQR strategy and the Decoupled PI controller. The system starts with CPL power

Preprints.org (www.preprints.org) | NOT PEER-REVIEWED | Posted: 5 April 2024 doi:10.20944/preprints202404.0433.v1

value CPL_1 = 0.5 W. At t = 43.6 s, the power value of CPL_1 becomes 0.7 W. It can be observed that when CPL_1 is connected, all the control efforts of loop 1 remain saturated, while the control effort of the Decoupled PI controller of loop 2 drops to a very low value. Although these control methods cannot compensate for the output errors caused by the CPL_1 perturbation (only the Decoupled PI controller can mitigate the steady-state error of V_2), they can ensure system stability and fast response.

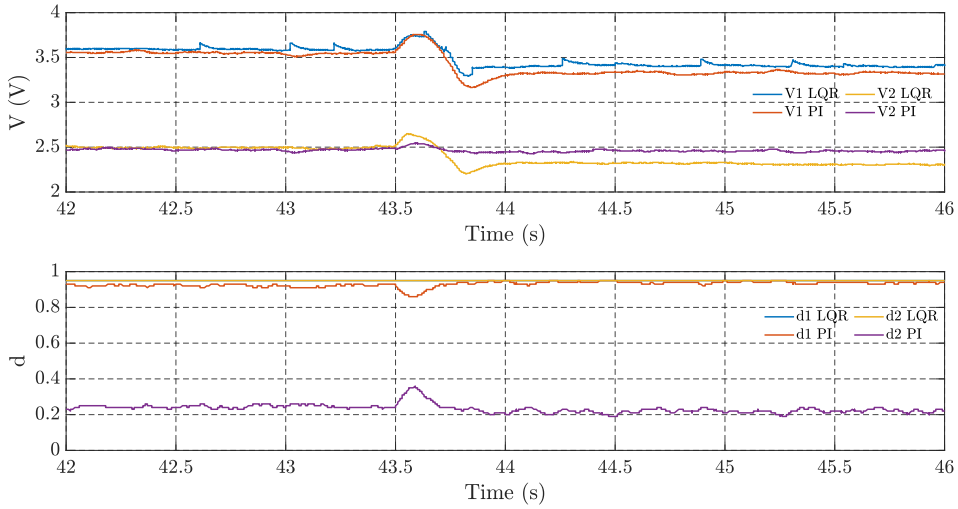

Figure 9. Experimental results for the test of power variation of the CPL_1 in output 1 of the single inductor dual output converter system, using LQR strategy and Decoupled PI structure.

Similar results are also obtained for the CPL_2 variation at output 2 for LQR strategy and Decoupled PI control structure, as shown in Figure 10, nevertheless, the Decoupled PI controller can compensate the oscillations in output 1 due to the power variation of the CPL_2. The system starts with a CPL power value of CPL_2 = 0.25 W, then at t = 54.8 s, the power value of the CPL_2 changes to 0.35 W. It can be observed that the control efforts of the loop 2 stay saturated when the CPL_2 is connected, on the other hand, the control effort of the Decoupled PI controller of the loop 2 falls to a very low value. Although, the control methodologies cannot compensate the error at the outputs due the perturbation in CPL_2 (only the Decoupled PI controller can mitigate the steady state error in V_1), but they can ensure the stability of the system with a quick response.

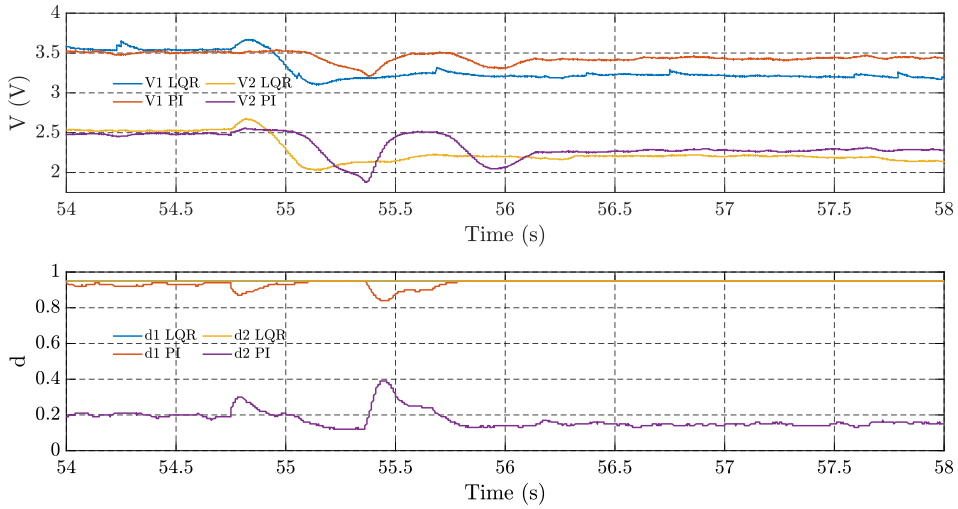

Figure 10. Experimental results for the test of power variation of the CPL_2 in output 2 of the single inductor dual output converter system, using LQR strategy and decoupled PI structure.

 doi:10.20944/preprints202404.0433.v1

Table 5 shows the ISE index for each output resulting from the CPL power change at output 1 for the LQR strategy and the Decoupled PI control structure. The ISE of the Decoupled PI controller is low for both outputs. Also, Table 6 shows the same indices for power variations in CPL at output 2, using the LQR strategy and the Decoupled PI control structure. The Decoupled PI approach has lower ISE values compared to the LQR strategy. These results show that the proposed Decoupled PI controller has significant performance improvements in this case and demonstrate its application in single-inductor-dual-output converter systems under such conditions.

Table 5. Values of the ISE and ISU indexes of the experimental data collected when the system submitted a parametric variation in the added CPL1.

Test	OUTPUT	ISE		ISU		J = ISE + ISU	
		LQR	PI	LQR	PI	LQR	PI
CPL1	V1	0.0525	0.0803	0.9025	0.8655	0.955	0.9458
	V2	0.0994	0.0553	0.9025	0.0545	1.002	0.1099

Table 6. Values of the ISE and ISU indexes of the experimental data collected when the system submitted a parametric variation in the added CPL2.

Test	OUTPUT	ISE		ISU		J = ISE + ISU	
		LQR	PI	LQR	PI	LQR	PI
CPL2	V1	0.1246	0.0546	0.9025	0.8796	1.027	0.9342
	V2	0.1500	0.1134	0.9025	0.0331	1.052	0.1465

6. Conclusions

This paper proposes the use of a robust LQR strategy and a Decoupled PI controller in a single-inductor dual-output DC-DC converter system to ensure robust stability and performance over the entire predetermined uncertain region, thereby reducing oscillations effects caused by the connection and variation of a constant power load, in parallel with a resistor of each converter output.

The proposed controllers have been exhaustively evaluated in physical experiments performed on a DC-DC SIMO converter board. The performances of the proposed methods, the LQR strategy, and the Decoupled PI structure are compared. Based on the experimental results, it is concluded that the proposed LQR strategy is able to maintain the required performance and reduce the steady-state errors V_1 and V_2 without excessive control effort or saturation of the duty cycle signals d_1 and d_2, which indicates good performance. On the other hand, when a CPL is connected to the outputs of the system, and it is subjected to a certain variation in the power of each CPL, both strategies are able to maintain the system stable, however, none of the controllers can mitigate the steady-state errors in V_1 and V_2 under these conditions. Thus, the results indicate that the proposed LQR strategy approach is reasonable and provides adequate performance improvements in the SIMO converter controls, offering robust performance and stability, while more research is needed to handle constant power loads (CPL). The authors are currently investigating strategies to deal with CPL, and results will be reported in future papers.

Author Contributions: Conceptualization, A.C.M.S., W.B.J. and R.L.P.d.M; methodology, W.B.J., R.L.P.d.M., and A.C.M.S., software, A.C.M.S. and A.S.G.; validation, A.C.M.S., W.B.J., R.L.P.d.M., and C.R.J.; formal analysis, A.C.M.S., W.B.J., R.L.P.d.M. and C.R.J.; investigation, A.C.M.S.; data processing A.C.M.S.; writing—original draft preparation, A.C.M.S.; writing—review and editing, A.C.M.S.; W.B.J. and R.L.P.d.M.

Funding: The first author of this paper acknowledges the support received from Conselho Nacional de Desenvolvimento Científico e Tecnológico (CNPq-Brazil), the Organization of American States (OAS) and the Coimbra Group of Brazilian Universities (GCUB).

Conflicts of Interest: The authors declare no conflicts of interest.

 doi:10.20944/preprints202404.0433.v1

References

1. Emadi A, Ehsani M. Multi-converter power electronic systems: definition and applications, In: Proceedings of the Power Electronics Specialists Conference, 2001. PESC. 2001 IEEE 32nd Annual, vol. 2. IEEE, 2001, pp. 1230–6.
2. A. Bhaumik, Y. Kumar, S. Srivastava, and M. Islam, ``Performance studies of a separately excited DC motor speed control fed by a buck converter using optimized PIλDμ controller,'' in Proc. Int. Conf. Circuit, Power Comput. Technol. (ICCPCT), Nagercoil, India, Mar. 2016, pp. 1-6.
3. M. Hassanalieragh, T. Soyata, A. Nadeau, and G. Sharma," UR-SolarCap: An open-source intelligent auto-wakeup solar energy harvesting system for supercapacitor-based energy buffering." IEEE Access, vol. 4, pp. 542-557, 2016.
4. D. Kumar, F. Zare, and A. Ghosh, "DC microgrid technology: System architectures, AC grid interfaces, grounding schemes, power quality, communication networks, applications, and standardizations aspects," IEEE Access, vol. 5, pp. 12230-12256, 2017.
5. H.-C. Chang and C.-M. Liaw, "An integrated driving/charging switched reluctance motor drive using three-phase power module," IEEE Trans. Ind. Electron., vol. 58, no. 5, pp. 1763-1775, May 2011.
6. M. I. Ghiasi, M. A. Golkar, and A. Hajizadeh, "Lyapunov based distributed fuzzy-sliding mode control for building integrated-DC microgrid with plug-in electric vehicle," IEEE Access, vol. 5, pp. 7746-7752, 2017.
7. X. Xiong, C. K. Tse, and X. Ruan, "Bifurcation analysis of standalone photovoltaic-battery hybrid power system," IEEE Trans. Circuits Syst. I, Reg. Papers, vol. 60, no. 5, pp. 1354-1365, May 2013.
8. Q. Xu et al., "A decentralized dynamic power sharing strategy for hybrid energy storage system in autonomous DC microgrid," IEEE Trans. Ind. Electron., vol. 64, no. 7, pp. 5930-5941, Jul. 2017.
9. X. Xiong, X. Ruan, H. Xi, and J. Ge, "Feed-forwarding the output voltage to improve efficiency for envelope-tracking power supply based on a switch-linear hybrid scheme," IEEE Trans. Power Electron., vol. 26, no. 8, pp. 2106-2111, Aug. 2011.
10. N. Mohan, T. M. Undeland, and W. P. Robbins, Power Electronics: Converters, Applications, and Design. Hoboken, NJ, USA: Wiley, 2002.
11. M. Salimi and A. Zakipour, "Direct voltage regulation of DC-DC buck converter in a wide range of operation using adaptive input-output linearization," IEEJ Trans. Elect. Electron. Eng., vol. 10, no. 1, pp. 85-91, Jan. 2015.
12. Dasika JD, Bahrani B, Saeedifard M, Karimi A, Rufer A. Multivariable control of single-inductor dual output buck converters. IEEE Trans Power Eletron Apr. 2014; 29(4). https://doi.org/10.1109/TPEL.2013.2266616.
13. Weiwei X, Xiaoting Z, Zhiliang H, Killat D. A single-inductor dual-output switching converter with average current mode control. J Semiconduct 2009; 30(9). https://doi.org/10.1088/1674-4926/30/9/095012.
14. Ma D, Ki WH, Tusi CY. A pseudo-CCM/DCM SIMO switching converter with freewheel switching. IEEE J Solid-State Circuits Jun. 2003;38(6):1007e14. https://doi.org/10.1109/JSSC. 2003.811976.
15. Kwon D, Rincon-Mora GA. Single-inductor multiple-output switching dc-dc converters. IEEE Trans. Circuits Syst. II Exp. Briefs Jul. 2009;56(8):614e8. https://doi.org/10.1109/TCSII.2009.2025629.
16. Trevisan D, Mattavelli P, Tenti P. Digital control of single-inductor multipleoutput step-down dc-dc converters in CCM. IEEE Trans Ind Electron Sep. 2008;55(9):3476e83. https://doi.org/10.1109/TIE.2008.921234.
17. Landau R., Barra W., Bessa I., Filho J.E., Ayres F., Neves C. Robust decentralized controller for minimizing coupling effect in single inductor multiple output dc-dc converter operating in continuous conduction mode. Jan. 2018; pp. 112–129. https://doi.org/10.1016/j.isatra.2018.01.006.
18. Le HP, Chae CS, Lee KC, Wang SW, Cho GH, Cho GH. A single-inductor switching dc-dc converter with five outputs and ordered power-distributive control. IEEE J Solid-State Circuits Dec. 2007;42(12):2706e14. https://doi.org/10.1109/JSSC.2007.908767.
19. Shen Z, Chang X, Wang W, Tan X, Yan N, Min H. Predictive digital current control of single-inductor multiple-output converters in CCM with low cross-regulation. IEEE Trans Power Electron Apr. 2012;27(4):1917e25. https://doi.org/10.1109/TPEL.2011.2168241.
20. Nayak, G., & Nath, S. (2020). Decoupled Voltage Mode Control of Coupled Inductor Single-Input Dual-Output Buck Converter. IEEE Transactions on Industry Applications, 1–1. doi:10.1109/tia.2020.2991650.
21. Wang, Y., Xu, J., & Yin, G. (2018). Cross Regulation Suppression and Stability Analysis of Capacitor Current Ripple Controlled SIDO CCM Buck Converter. IEEE Transactions on Industrial Electronics, 1–1. doi:10.1109/tie.2018.2838103.
22. Dong, Z., Li, X. L., Tse, C. K., & Zhang, Z. (2020). Derivation of Single-Input Dual-Output Converters With Simple Control and No Cross Regulation. IEEE Transactions on Power Electronics, 35(11), 11930–11941. doi:10.1109/tpel.2020.2983618.
23. Zhou, S., Zhou, G., Liu, G., & Mao, G. (2020). Small-signal Modeling and Cross-regulation Suppressing for Current-mode Controlled Single-inductor Dual-output DC-DC Converters. IEEE Transactions on Industrial Electronics, 1–1. doi:10.1109/tie.2020.2996139.

 doi:10.20944/preprints202404.0433.v1

24. NAYAK, G., & Nath, S. (2020). Decoupled Average Current Control of Coupled Inductor Single Input Dual Output Buck Converter. IEEE Journal of Emerging and Selected Topics in Industrial Electronics, 1–1. doi:10.1109/jestie.2020.3014833.
25. Shekel J. Nonlinear problems in the design of cable-powered distribution networks. IEEE Transactions on Cable Television 1976, pp. 11–7.
26. Hodge C, Flower J, Macalindin A. Dc power system stability. In: Proceedings of the IEEE Electric Ship Technologies Symposium, 2009. ESTS 2009, pp. 433–9.
27. Rivetta, C.;Williamson, G.A.; Emadi, A. Constant power loads and negative impedance instability in sea and undersea vehicles: Statement of the problem and comprehensive large-signal solution. In Proceedings of the IEEE Electric Ship Technologies Symposium, Philadelphia, PA, USA, 27 July 2005, pp. 313–320.
28. Ghisla, U.; Kondratiev, I.; Dougal, R. Protection of medium voltage DC power systems against ground faults and negative incremental impedances. In Proceedings of the IEEE SoutheastCon 2010 (SoutheastCon), Concord, NC, USA, 18–21 March 2010, pp. 259–263.
29. Suresh, S.; Aditya, R.;Deepak, F. Constant power loads and their effects in DC distributed power systems: A review. In: Renewable and Sustainable Energy Reviews, 2017, pp. 407-421.
30. K. E. L. Marcillo et al. Interval robust controller to minimize oscillations effects caused by constant power load in a DC multi-converter buck-buck system, IEEE Access, vol. 7, Feb. 2019, pp. 2632426342.
31. Xiong Q, Wen-Jian C. Effective transfer function method for decentralized control system design of multi-input multi-output processes. Journal of Process Control Sep. 2006;16:773-84. https://doi.org/10.1016/j.jprocont.2006.04.001.
32. Lin K, Huang C, Chen D, Liu KH. Modeling and design of feedback loops for a voltage-mode single-inductor dual-output buck converter. In: IEEE PESC - power electronics specialists conference; Jun. 2008. https://doi.org/10.1109/PESC.2008.4592479.
33. Xiong Q, Wen-Jian C. Effective transfer function method for decentralized control system design of multi-input multi-output processes. J Process Control Sep. 2006;16:773e84. https://doi.org/10.1016/j.jprocont.2006.04.001.
34. Xiong Q, Wen-Jian C, Mao-Jun H. A practical loop pairing criterion for multivariable processes. J Process Control Oct. 2005;15:741e7. https://doi.org/10.1016/j.jprocont.2005.03.008.
35. L. Castro, L. Cunha, B. Dutra and A. Silveira, "Digital lqg controller design applied to an electronic system", IEEE Latin America Transactions, vol. 18, no. 03, pp. 581-588, 2020.
36. Hespanha, J. P. (2018, February 13). Linear Systems Theory. Princeton University Press.
37. Pérez, P. A., Albertos, P., Sala, D. A., & Antonio, S. (2004, January 1). Multivariable Control Systems. Springer Science & Business Media.
38. Skogestad, S., & Postlethwaite, I. (2005, November 4). Multivariable Feedback Control. John Wiley & Sons.
39. Stevens, B. L., Lewis, F. L., & Johnson, E. N. (2015, October 2). Aircraft Control and Simulation. John Wiley & Sons.
40. K. J. Aström and T. Hägglund. PID Controllers: Theory, Design, and Tuning. Instrument Society of America, Research Triangle Park, NC, 1995.
41. K. J. Aström, K. H. Johansson, and Q. Wang. Design of Decoupled PID Controllers, for MIMO Systems. In: Proceedings of the American Control Conference, Arlington, VA, USA, 27 June 2001, pp. 2015-2020.
42. Erickson RW, Maksimovic D. Fundamentals of power electronics. 2 Edition. Kluwer Academic Publishers; 2001.